Universal transport coefficient behaviour in ionic melts

1999 J. Phys.: Condens. Matter 11 8773

(http://iopscience.iop.org/0953-8984/11/45/302)

J. Phys.: Condens. Matter **11** (1999) 8773–8784. Printed in the UK PII: S0953-8984(99)05577-0

Universal transport coefficient behaviour in ionic melts

E Veliyulin†, E Shasha†, A Voronel†, V Sh Machavariani†, Sh Seifer†, Yu Rosenberg‡ and M G Shumsky§

† School of Physics and Astronomy, Raymond and Beverly Sackler Faculty of Exact Sciences, Tel-Aviv University, 69978, Tel-Aviv, Israel
‡ Wolfson Centre for Materials Research, Tel-Aviv University, Ramat Aviv 69978, Israel
§ Graduate Center for Materials Research, University of Missouri–Rolla, Rolla, MO 65401, USA

Received 28 June 1999

Abstract. Precise resistivity and viscosity measurements for ionic mixed melts, regular and glass-forming, have been performed on the liquid state over a wide range of viscosity variation. Their universal behaviour in the high-temperature region allows us to scale them relative to their activation energy. The resistivity–viscosity relation reveals a fractional-power character over the whole range of parameters investigated. This interdependence suggests a fractional character of the Stokes–Einstein law of the viscosity–diffusion relation for ions in melts.

1. Introduction

In our previous papers [1, 2] a universal behaviour of the viscosity for a variety of ionic melts was demonstrated over a wide range of parameters. Although the conductivity has been extensively measured before [3], we still lack systematic data for a wide range of temperature to compare with the viscosity. While for the usual simple melts the resistivity seems to be roughly proportional to the viscosity, this ceases to be the case over the wider range of parameters which is achievable for mixed melts. We have performed a series of precise resistivity measurements for ionic mixed melts with low melting points to allow comparison with the corresponding viscosity data. In particular, mixtures exhibiting a trend to glassification have been chosen, to considerably stretch the range of the parameters achievable within the liquid state. The nitrate melts $NaNO_3$, $RbNO_3$, KNO_3, $Ca(NO_3)_2$ and their mixtures exhibit viscosities amenable to precise measurement over a wide but convenient range of temperature. Mixing these salts enables one to prepare samples of different glass-forming abilities depending on the composition. This also provides the opportunity to compare the results with our previous viscosity and optical measurement data [2, 4]. For comparison, we have also measured the resistivity of a $(KCl)_{0.33}(AlBr_3)_{0.67}$ mixture and a glass-forming LiCl–water solution. A variety of data from the literature [5–7] have been considered, to test the generality of our approach.

2. Experimental procedure

Ultrapure KNO_3 and $Ca(NO_3)_2{\cdot}4H_2O$ (Alpha Corporation), $NaNO_3$ (99.995%), $RbNO_3$ (99.7%) and $AlBr_3$ (99.99%) (Aldrich Corporation), LiCl (99+%) (Merck) and KCl (99.9%) (Johnson–Matthey) components were used for sample preparation. In order to obtain pure $Ca(NO_3)_2$ salt, crystallohydrate crystals of $Ca(NO_3)_2{\cdot}4H_2O$ were slowly heated under vacuum

0953-8984/99/458773+12$30.00

up to 150 °C and kept at this temperature for more than five hours. The dehydration procedure was additionally controlled by sample weight registration. The alkali nitrate crystals were dried under vacuum at 150 °C for several hours. The dry components $NaNO_3$, KNO_3, $RbNO_3$ and $Ca(NO_3)_2$ were treated in a glove box under a controlled nitrogen atmosphere, weighed out and mixed. The ready-mixed sample was put into a hermetically closed measuring cell.

Our resistivity measurements were performed by a two-terminal AC technique with a Hewlett-Packard 4284A precision LCR meter (20 Hz–1 MHz). The lower part of the measuring cell consists of a calibrated glass tube (with an internal diameter 0.339 ± 0.001 cm) with two welded electrodes (0.3 mm diameter Pt wire) at a distance 8.00 ± 0.05 cm from each other.

After melting it within the measuring cell, the sample was kept at the highest-temperature point in a liquid state for about ten hours to enable complete mixing of the components and, thus, to ensure the stability of the measured impedance. Then it was cooled down at a constant rate (50 K h^{-1}) and the impedance was measured as a function of temperature at seven different frequencies (1, 5, 10, 50, 100, 500 and 1000 kHz). The system was fully monitored by a personal computer through the GP-IB bus and RS-232 serial port. The temperature was measured by a Pt versus Pt + 10%Rh thermocouple with a reference junction and controlled by a Eurotherm programmable controller.

An equivalent circuit consisting of four elements was constructed (figure 1) to simulate the measured impedance. These four elements are: a resistor R_s simulating the DC bulk resistance of a sample; a contact capacitance C_{cont} simulating the AC electrode polarization effect; and two parasitic elements—a coil L_p and capacitance C_p—representing the inductance and capacity of the measuring cell itself. The bulk resistance of the sample R_s was extracted from the measured impedance by solving numerically a set of equations derived from the proposed circuit of figure 1 for (at least) five different frequencies. The resistivity was deduced afterwards from the resistance data and the geometrical parameters of the cell.

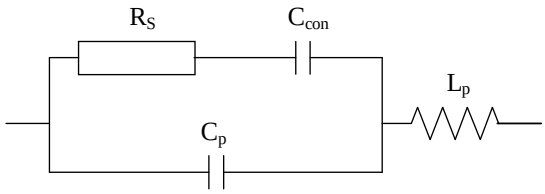

Figure 1. The equivalent circuit of the resistivity measurement scheme: R_s is a resistor simulating the DC bulk resistance of the sample; C_{cont} is a contact capacitance simulating the AC electrode polarization effect; L_p and C_p are the inductance and capacitance of the measuring cell itself.

3. Phase diagrams

Knowledge of a mixture's phase diagram is important because it makes it possible to determine the positions of the melting points, and therefore also the crystallization trend of the sample, in a preliminary fashion. As a rule, the diagrams for the states reported by reference [3] are reliable. However, the $RbNO_3$–$NaNO_3$ diagram reported in [3] to exhibit unlimited solubility in the solid state looks doubtful.

Indeed, our thermophysical and our x-ray diffraction studies gave evidence of a different kind of phase diagram for $RbNO_3$–$NaNO_3$, which is presented in figure 2. The liquidus line temperatures (and in fact those of the solidus line too, but with less certainty) were detected from abrupt changes of density [1] and conductance for different compositions of this system.

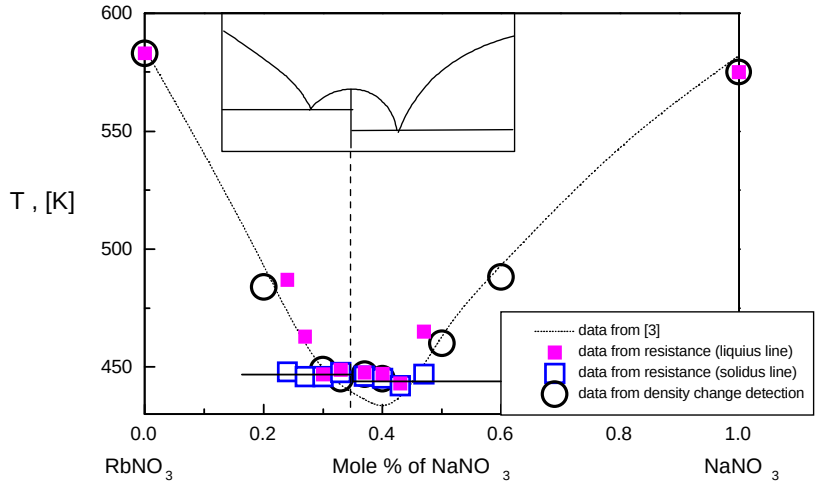

Figure 2. The phase diagram of $RbNO_3$–$NaNO_3$. The inset shows schematically the form of the diagram in the region of concentrations from 0.28 to 0.43 for $NaNO_3$.

The x-ray diffraction study of the solid–liquid phase transition for the $Rb_{0.6}Na_{0.4}NO_3$ composition was performed with Cu Kα radiation on a Θ:Θ 'Scintag' powder diffractometer equipped with a liquid-nitrogen-cooled intrinsic-Ge solid-state detector. In figure 3, one can

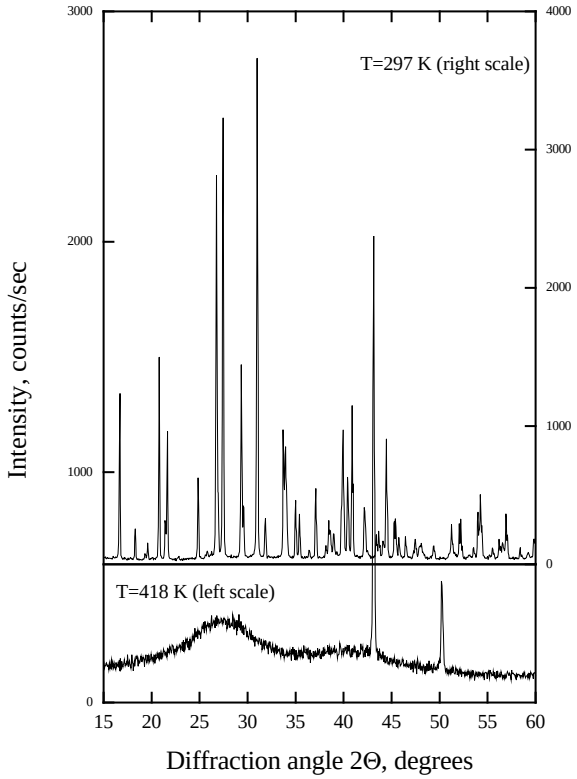

Figure 3. X-ray diffraction patterns for the $Rb_{0.6}Na_{0.4}NO_3$ composition at different temperatures: the upper part which corresponds to $T = 297$ K coincides with the pattern of the stoichiometric crystalline phase $Rb_2Na(NO_3)_3$ (see reference [8]); the lower part corresponds to the liquid state at $T = 418$ K.

see the two diffraction patterns obtained from $Rb_{0.6}Na_{0.4}NO_3$ at about its melting (supercooled) temperature and at room temperature. While the former indicates the undercooled liquid state, the latter pattern clearly indicates the existence of a new stoichiometric phase, $Rb_2Na(NO_3)_3$, which has been reported once before as a result of a hydride solution investigation in [8]. The presence of this stoichiometric compound confirms the existence of a maximum between the two minima at the bottom of the diagram in figure 2. Thus, in spite of the fact that $RbNO_3$ and $NaNO_3$ are no different as regards their cationic charge, their mixture probably contains some complex ions.

4. Resistivity data

The precise resistivity measurements were performed for nitrate melts in the range from roughly 740 K down to the crystallization points (about 400–500 K). In the cases of glass-formers, we were able to extend our to measurements well below this. For LiCl–water solutions, a few concentrations were investigated in the range from room temperature down to roughly 180 K.

To analyse our resistivity data, one can use an exponential formula (the so-called Arrhenius formula), as was done before for our viscosity data [1, 2]:

$$\rho/T = B_\rho \exp(E_\rho/T). \tag{1}$$

Table 1 contains the parameters of equation (1) together with the values derived in an analogous way from the viscosity data [1, 2]. Although in a low-temperature region the data deviate considerably from the Arrhenius form, it still makes sense to use this form, since the activation energy E_ρ (in kelvins) provides a reasonable temperature scale for the melts investigated. Figure 4 illustrates this for many melts (including ZBLAN20: $0.53ZrF_4$–$0.20BaF_2$–$0.04LaF_3$–$0.03AlF_3$–0.20NaF; see reference [7]) in an Arrhenius plot ($\lg(\rho/B_\rho T)$ versus E_ρ/T). Unfortunately, for both $(KCl)_{0.33}(AlBr_3)_{0.67}$ and the LiCl–water solutions there is no high-temperature region, but the 'corresponding-states law' based on scaling with E_ρ is still valid.

Table 1. Parameters of the Arrhenius formula for the resistivity (B_ρ and E_ρ) and the viscosity [1, 2] (B_η and E_η) high-temperature data. The ratio of activation energies E_ρ/E_η is also presented. The missing data for some of the melts have been taken from references [3, 5, 6, 7].

Salt	B_ρ (Ω cm K^{-1})	E_ρ (K)	B_η (cP K^{-1})	E_η (K)	E_ρ/E_η
$LiNO_3$	3.55×10^{-5}	2200	4.59×10^{-5}	2920	0.75
$NaNO_3$	5.11×10^{-5}	2050	6.14×10^{-5}	2570	0.80
$KNa(NO_3)_2$	5.18×10^{-5}	2230	5.21×10^{-5}	2660	0.84
KNO_3	5.21×10^{-5}	2390	3.95×10^{-5}	2930	0.81
$RbNO_3$	6.27×10^{-5}	2470	5.59×10^{-5}	2790	0.89
$CsNO_3$	8.71×10^{-5}	2370	2.73×10^{-5}	3360	0.71
$AgNO_3$	6.81×10^{-5}	1830	8.86×10^{-5}	2310	0.80
$Rb_3Na_2(NO_3)_5$	5.79×10^{-5}	2400	5.48×10^{-5}	2710	0.89
$Ca_2K_3(NO_3)_7$	6.66×10^{-5}	2720	(6.00×10^{-5})	(3130)	(0.87)
$Ca_2Rb_3(NO_3)_7$	7.23×10^{-5}	2850	4.35×10^{-5}	3400	0.84
$Ca_3Na_1Rb_6(NO_3)_{13}$	8.58×10^{-5}	2580			
$(LiCl)_{0.16}(H_2O)_{0.84}$	3.55×10^{-5}	1890	(0.29×10^{-5})	(2460)	(0.77)
ZBLAN20	0.96×10^{-5}	5130	2.85×10^{-5}	5910	0.87

In accordance with equation (1), the scaled conductivity ($B_\rho E_\rho/\rho$) can be presented as a universal function of a single variable T/E_ρ only:

$$\frac{B_\rho E_\rho}{\rho} = \frac{E_\rho}{T}\exp\left(-\frac{E_\rho}{T}\right). \tag{2}$$

Figure 5, which presents the data as a function of the scaled temperature T/E_ρ, illustrates the universality of equation (2) rather convincingly. However, in the low-temperature region (where, roughly, $T/E_\rho < 0.2$) the glass-formers deviate from the universal graph. One can accept this as a definition of 'high'- and 'low'-temperature regions.

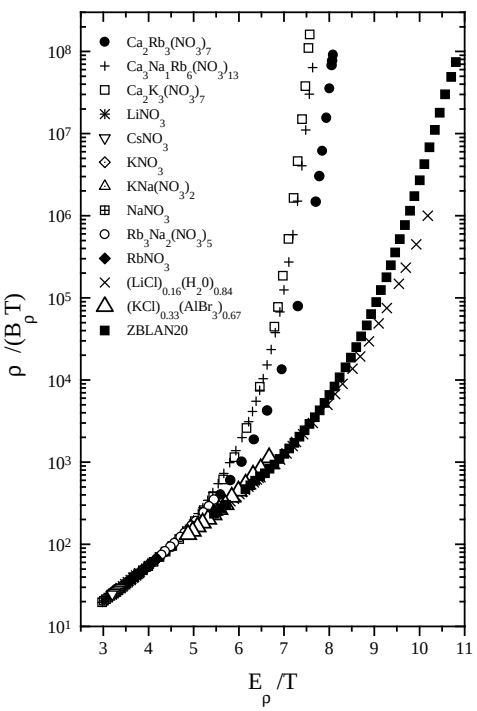

Figure 4. The scaled resistivities of ionic melts as functions of the inverse scaled temperature in a semi-logarithmic plot.

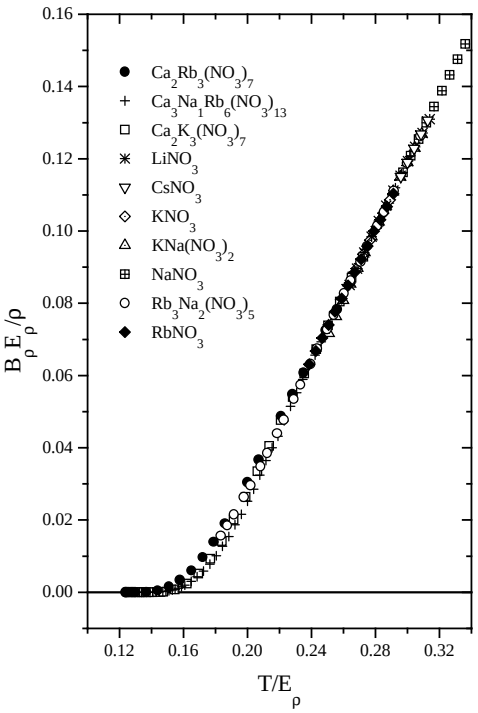

Figure 5. The scaled conductivities of ionic melts as functions of the scaled temperature.

The experimental conductivity data above $T/E_\rho > 0.2$ look like a linear function of temperature. This is not in contradiction with equation (1). Indeed, the function on the right-hand side of equation (2) has an inflection point at

$$T/E_\rho = (2-\sqrt{2})/2 \approx 0.293.$$

In the vicinity of this point, the function actually behaves almost linearly. This leads empirically to the linear dependence of the conductivity on the temperature for the majority of melts (this makes the experimental data compatible with 'free-volume' concepts [9]). It is particularly the case for the nitrates, since the point $T/E_\rho = 0.293$ corresponds for them to the middle of the temperature range available for the measurements [10].

As one can see from figure 4, the data in the low-temperature region, halfway to glassification, are not properly scaled by an Arrhenius formula with two fitting parameters.

This is why many authors use a Vogel–Fulcher empirical formula with three parameters [11] to present their data on glass-forming melts. The Vogel–Fulcher equation was presented by Angell in the following form [12]:

$$\rho = C_\rho \exp\left(\frac{D_\rho T_{0\rho}}{T - T_{0\rho}}\right) \tag{3}$$

where D_ρ is defined as a fragility coefficient and T_0 is a characteristic constant identified by some authors with the Kauzmann point [13]. The coefficient D_ρ is greater for the stronger glasses.

The parameters (C_ρ, D_ρ and $T_{0\rho}$) of the Vogel–Fulcher equation for our resistivity data over the full range of our measurements are presented in table 2.

Table 2. The parameters (C_ρ, D_ρ and $T_{0\rho}$) of the Vogel–Fulcher equation for our resistivity data (see equation (4)) together with the parameters (C_η, D_η and $T_{0\eta}$) of the Vogel–Fulcher equation for viscosity (see references [1, 2]). The parameters D_ρ, C_ρ and $T_{0\rho}$ for ZBLAN20 were obtained by fitting over the high-temperature region ($T > 500$ K). The ratio of the fragility coefficients D_ρ/D_η is also presented. The missing data for some of the melts have been taken from references [3, 5, 6, 7].

Salt	C_ρ (Ω cm)	D_ρ	$T_{0\rho}$ (K)	C_η (cP)	D_η	$T_{0\eta}$ (K)	D_ρ/D_η
$Rb_3Na_2(NO_3)_5$	0.277	2.90	240	0.292	3.69	232	0.79
$Ca_2K_3(NO_3)_7$	0.344	2.15	317	0.220	2.72	320	0.79
$Ca_2Rb_3(NO_3)_7$	0.471	2.28	307	0.411	3.09	294	0.74
$Ca_3Na_1Rb_6(NO_3)_{13}$	0.441	2.27	295				
$Ca_2Na_2Rb_6(NO_3)_{12}$	0.472	1.94	291				
$(KCl)_{0.33}(AlBr_3)_{0.67}$	0.807	3.05	200	0.388	2.64	226	0.87
$(LiCl)_{0.16}(H_2O)_{0.84}$	0.198	4.16	135	0.034	6.34	123	0.66
ZBLAN20	0.036	5.86	376	0.041	5.38	458	1.09

5. Viscosity data

The viscosity data for some of our melts were measured in earlier work [1, 2]. But CRN ($Ca_2Rb_3(NO_3)_7$) glass-former viscosity measurements have been performed recently, for comparison with our resistivity data. Figure 6 presents our viscosity data together with data from the literature in an Arrhenius plot analogous to that of figure 4 for the resistivity. One can see that 'the corresponding-states law' is valid also for viscosity if the temperature is similarly scaled relative to the corresponding E_η. At low temperature the viscosity behaviour of the melts is becoming material dependent, as also happens for the resistivity. Both the Arrhenius and the Vogel–Fulcher equation parameters have been tabulated in tables 1 and 2. In the last column of each table the ratios of the activation energies, E_ρ/E_η, or fragility coefficients, D_ρ/D_η, are presented (E_ρ and D_ρ are derived from the resistivity data; E_η and D_η are derived from the viscosity data). They appear to be in unexpectedly good agreement. However, a comparison of figures 4 and 6 shows that one additional parameter D_η ('fragility') is not enough to characterize the difference in glass-forming behaviour.

6. The resistivity–viscosity relation

The universal high-temperature behaviour of the resistivity (figure 4) and viscosity (figure 6), on one hand, and the close ratios of the activation energies E_ρ/E_η and fragility coefficients

D_ρ / D_η (table 2), on the other hand, allow us to check the resistivity–viscosity interdependence straightforwardly.

As a result of our extended study of both electrical conductivity and viscosity, we are able to consider the functional interdependence of these two quantities directly, without any use of approximating formulae (Arrhenius or Vogel–Fulcher).

Figure 7 presents our experimental data for ionic melts in a log–log plot. The frequently used combination of the Stokes–Einstein (SE) law [14, 15] for Brownian motion and the Nernst–Einstein (NE) law [14, 15] for ionic conductivity requires a linear resistivity–viscosity dependence. Thus the slope of the resistivity–viscosity curve in a log–log plot is expected to be equal to 1. However, the slope in figure 7 is in fact obviously less than 1 and roughly the same ($m \approx 0.8 \pm 0.1$) for all of the melts investigated over the wide viscosity range starting from viscosity 10^{-3} cP. Therefore the fractional conductivity–viscosity relation can be written for a rather wide range of viscosity variation as follows:

$$\frac{\rho}{T} \propto \left(\frac{\eta}{T}\right)^m. \tag{4}$$

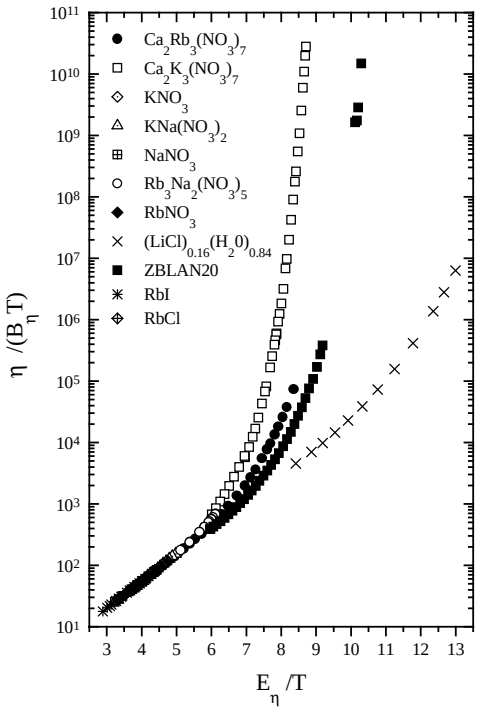

Figure 6. The scaled viscosities of the ionic melts as functions of the inverse scaled temperature in a semi-logarithmic plot.

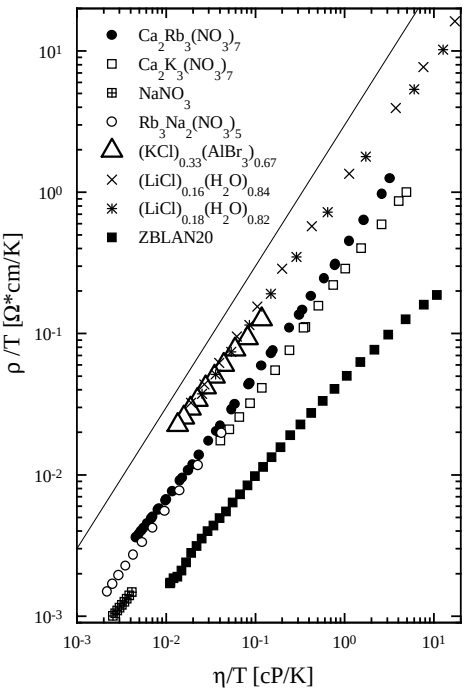

Figure 7. ρ/T as a function of η/T in a log–log plot for different ionic melts and solutions. The solid line corresponds to the slope m equal to 1.

We note that the temperature factor T, which is insignificant for the glassification region, is rather important for the high-temperature part of the dependence. The numerical value m from equation (4) is in a good agreement with the values of the ratio E_ρ / E_η derived for the high-temperature region (see table 1). This confirms the intrinsic character of the high-temperature parameters E_ρ and E_η and equation (4).

The phenomenological fractional relation (4) may be interpreted as a manifestation of a fractional relation between the individual ion's mobility and the viscosity of the medium as a whole. This means assuming the fractional Stokes–Einstein (FSE) law to apply to microscopic particles: $D \propto (\eta/T)^m$ [16]. It agrees well with the straightforward measurements of the translational diffusion coefficients of tracer molecules within viscous media [17, 18]. The experimental data of [18] cover, in fact, 14 orders of viscosity variation but, unfortunately, the authors used η as a variable rather than η/T, and thus received the impression that the fractional law was valid only asymptotically close to the glassification limit.

Since for the index determination in a log–log plot the range of magnitude is particularly important, the cases of the glass-formers $Ca_2K_3(NO_3)_7$ and the LiCl–water solution are presented separately in figure 8, together with the experimental data on ZBLAN20 [7] melt. This figure explicitly shows the non-linear character of the conductivity–viscosity relation over fourteen orders of magnitude of viscosity variation. The exponent m varies in this range between 0.9 and 0.5, decreasing in the glassification region.

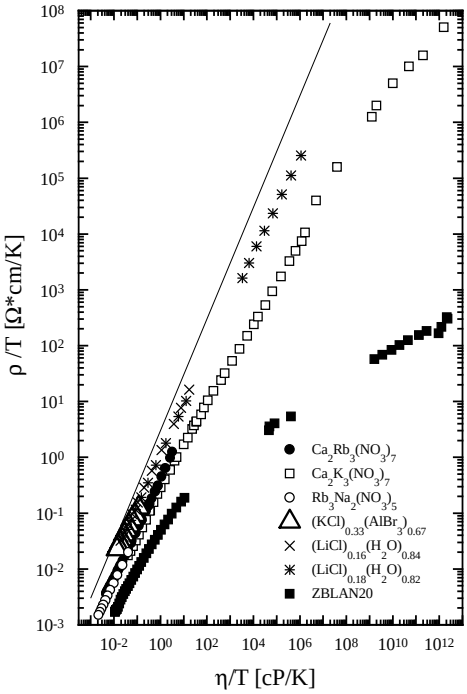

Figure 8. ρ/T as a function of η/T in a log–log plot for different ionic melts and solutions for 14 orders of magnitude of viscosity variation. The solid line corresponds to the slope m equal to 1.

Thus the log–log viscosity–conductivity plotting represents a both non-trivial and *model-independent* way to characterize the transport properties of melts. While the exponent m in equation (4) is not actually universal, its deviation from universality is material dependent. One can expect new physical information to be derived from this dependence.

7. Discussion

The 'corresponding-states law' established in this work (see figures 4, 5 and equation (2)) allows us to properly define the 'high'- and 'low'-temperature regions. While the high-temperature behaviour of melts can be scaled with energetic characteristics E_ρ, the low-temperature behaviour ($T/E_\rho \leqslant 0.2$) requires additional parameters.

If one assumes the translational diffusion to be the main mechanism of charge transport in the high-temperature region of a simple melt, the conductivity activation energy E_ρ roughly characterizes the mobility of the ions. However, an elementary viscous-flow process should include more than an individual ion's motion. Therefore, its activation energy E_η even at high temperature cannot be the same as that for mass (or charge) transport. This leads to the deviation of the exponent m from 1 in equation (4).

In spite of the fact that empirical data supporting equation (4) appeared as early as 1908 [19], the quasihydrodynamic approximation ($m = 1$) to molecular motion based on the Stokes–Einstein formula for Brownian particles remained widely used [14]. Indeed, the frictional resistance to the motion of an individual Brownian (macroscopic) particle has been supposed to be proportional to the viscosity of the medium, since its velocity is small relative to stochastic atomic motions. However, this assumption cannot be correct for the diffusion of the ions themselves, since they move with the same thermal velocity as the atoms of the medium. Recent computer simulations of glass-forming systems [20, 21] have demonstrated explicitly a fractional-power relation analogous to equation (4). The relaxation time τ_α calculated in reference [20] (which is proportional to η/T) and the self-diffusion time $\propto 1/D$ (proportional to the reciprocal of ρ/T for a one-component fluid) above the mode-coupling critical point (MCT) [22] T_c are connected non-linearly:

$$\tau_\alpha \propto (1/D)^m. \tag{5}$$

The estimations in reference [20, 21] of m give values from 0.7 to 0.82, which is very close to the empirical value $m = 0.8 \pm 0.1$ derived from our measurements [16] for the region of comparatively high temperature far from the glassification point (see figure 7).

At lower temperature, the corresponding-states law fails to be valid (see figure 4) and the exponent m has a tendency to decrease near the glassification point (see figure 8, covering a wider range of viscosity). This behaviour is analogous to that observed by Andreozzi *et al* [23] for rotational diffusion in a glassifying liquid. One can see that this m changes differently for different glass-formers.

Let us try to probe deeper in our attempt to understand the nature of supercooled fluid. The concept of a sort of heterogeneity in the supercooled system is the key idea of many recent theories [24–28]. Whatever the reason for the emergence of this heterogeneity, the corresponding liquid on its nanometric scale can be presented as a composite material with inclusions of greater rigidity (and, probably, of higher density) [29,30], which live much longer than the reorientation time of an individual molecule [30].

The conductivity of a composite material consisting of two components (or phases) of different conductivity (assuming for simplicity the rigid phase to be an insulator—i.e. its conductivity to be close to zero) can to a first approximation (the 'effective-medium approximation' (EMA) [31]) be presented as

$$\sigma_{\text{eff}} = \sigma_1[1 - p_2(T)/p_c']. \tag{6}$$

Here, σ_{eff} is a measured quantity, σ_1 is the conductivity of the fluid phase, $p_2(T)$ is the volume fraction of the rigid (insulating) phase, which depends on the temperature. This dependence is specific to different glass-formers. Linearity of equation (6) is possible until p_2 is small compared to p_c'; this is connected with a threshold determined by the geometry of the inner composite structure. For p_2 close to the threshold value, the right-hand side of equation (6) transforms into a complicated function of the inner structure of the material, which has to be carefully investigated.

For the fluidity φ ($\varphi = 1/\eta$) of the composite, the analogous formula can be written [32] as

$$\varphi_{\text{eff}} = \varphi_1[1 - p_2(T)/p_c'']. \tag{7}$$

Until $p_2(T) \ll 1$, the volume fraction p_2 in equation (7) can be considered the same (or, one hopes, close to the same) as in equation (6), since the clusters which are mechanically rigid have to be insulating as well. However, p_c' and p_c'' for equation (6) and equation (7) may be essentially different.

One has to remember that though we use the terms 'phase' and 'component', the above-mentioned inhomogeneities are not thermodynamically stable. These stochastically emerging (and disappearing) closer-packed bodies [20, 21, 32, 33] create walls and chains rather than the compact three-dimensional regions. That is why the limiting figures p_c' and p_c'' might be considerably different from the figures expected from percolation theory [34].

Since one observes for the liquid the universal Arrhenius behaviour in the high-temperature region of figure 4, where it is actually homogeneous, it is natural to extrapolate this behaviour for the fluid phase (σ_1 and φ_1) down to the supercooled region in accordance with equation (1) and its analogy for viscosity.

Thus, until the term $p_2(T)/p_c'$ (the collective obstruction effect of the rigid inclusions) is small compared to 1 (and the index m is not much less than 1), the relation between the conductivity and fluidity is weakly dependent on the temperature and is determined mostly by the high-temperature behaviour of the liquid (see figure 7). The deviation from universality may grow with the growing $p_2(T)/p_c'$ term, as is clear from figure 8 where the curves for different glass-formers deviate from their parallelism at lower temperature. The fact that the exponent m is less than 1 (so-called 'decoupling') is frequently interpreted [30] as a manifestation of a trend towards glassification. But figure 7 rather convincingly demonstrates an intrinsic character of the resistivity–viscosity 'decoupling' or, perhaps it is better to say, the generality of the fractional (FSE) relation (4) between them. The trend towards glassification leads to further reduction of m depending on the individual character of a glass-former determined by the specific geometry of the clusters which it forms.

Figure 9 presents the deviations of the effective conductivity and fluidity ($(\sigma_1-\sigma_{\text{eff}})/\sigma_1 = p_2(T)/p_c'$ and $(\varphi_1-\varphi_{\text{eff}})/\varphi_1 = p_2(T)/p_c''$, respectively) from those of the 'fluid phase'; these originate from the presence of 'rigid' inclusions. In a first approximation, the conductivity

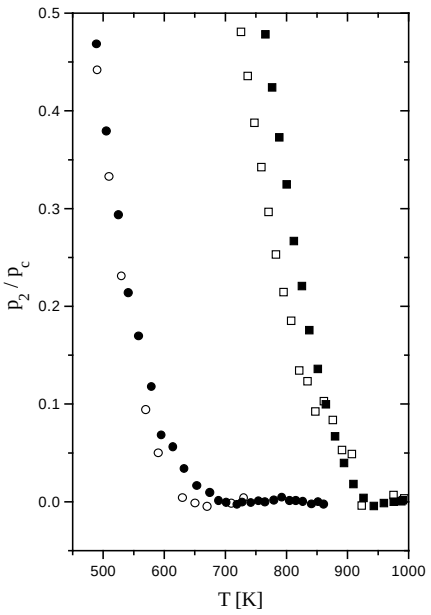

Figure 9. Deviations from the 'fluid-phase' conductivity and fluidity of the effective conductivity $(\sigma_1-\sigma_{\text{eff}})/\sigma_1 = p_2(T)/p_c'$ (empty symbols) and fluidity $(\varphi_1-\varphi_{\text{eff}})/\varphi_1 = p_2(T)/p_c''$ (filled symbols) as functions of temperature. Circles correspond to $Ca_2Rb_3(NO_3)_7$ and squares to ZBLAN20 data.

and the viscosity of CRN glass-former give close results. But the stronger decoupling of the conductivity and viscosity data observed for ZBLAN20 by Hasz *et al* [7] (see figure 8) reveals a considerable difference between the individual ionic motions and the collective viscous flow even within the range of validity of the EMA. The increase of $p_2(T)$ towards the glassification point probably leads to strong deviations from linearity in both equations (6) and (7). While for the viscous flow the establishing of an interconnected infinite cluster of the rigid phase is important ($p_2 < 0.5$), for the conductivity the important limit is the loss of the infinite cluster of the fluid phase ($[1 - p_2] < 0.5$). The accuracy of phenomenological measurements is not sufficient to allow a detailed judgment to be made as regards the shape of the rigid inclusions. But further investigation may produce a meaningful classification of glass-formers in accordance with the discrepancy between the parameters derived from the conductivity and viscosity data.

8. Conclusions

Precise resistivity data have been obtained for the ionic pure and mixed melts $RbNO_3$, $NaNO_3$, $Rb_3Na_2(NO_3)_5$, $Ca_2K_3(NO_3)_7$, $Ca_2Rb_3(NO_3)_7$, $Ca_3Na_1Rb_6(NO_3)_{13}$, $(KCl)_{0.33}(AlBr_3)_{0.67}$ and LiCl–water solutions over a wide range of parameters distant from the glassy state.

These results, together with the data from the literature, allow us to find universal features in the melt resistivity behaviour which were observed before for viscosity [1,2]. The conductive behaviour of the melts in the high-temperature region is found to be a universal function of the scaled temperature (the 'corresponding-states law'). The activation energy E_ρ derived from the Arrhenius equation has been suggested as a scaling parameter. The parameters for all of the melts have been tabulated and compared with those derived from viscosity.

In the low-temperature region, which is defined by $T/E_\rho < 0.2$, the universal diffusion mechanism of transport fails and the effects of the inhomogeneity of the undercooled liquid are revealed to be important. The Vogel–Fulcher equation, which takes these effects into account phenomenologically, requires the introduction of an additional characteristic 'fragility' parameter, D_ρ.

The viscosity–resistivity relation derived from our experimental data appears to be a fractional-power function which is valid over a much wider range than the corresponding-states law.

The preliminary consideration of an intrinsic heterogeneity of two different undercooled glass-formers is presented.

Acknowledgments

This work was partially supported by the German–Israeli Foundation (GIF) for Science and Development. This work was also supported by The Aaron Gutwirth Foundation, Allied Investments Limited (Israel). The authors are grateful to Dr W C Hasz for his kind readiness to provide us with the experimental data on ZBLAN20 melt.

References

[1] Veliyulin E, Voronel A and Oye H A 1995 *J. Phys.: Condens. Matter* **7** 4821
[2] Voronel A, Veliyulin E, Grande T and Oye H A 1997 *J. Phys.: Condens. Matter* **9** L247
[3] Janz G J, Krebs U, Siegenthaler H and Tomkins R 1972 *J. Phys. Chem. Ref. Data* **1** 588
[4] Kisliuk A, Loheider S, Sokolov A, Soltwisch M, Quitmann D, Shasha E and Voronel A 1995 *Phys. Rev.* B **52** 13 083
[5] Moynihan C T, Bressel R D and Angell C A 1971 *J. Chem. Phys.* **55** 4414

Moynihan C T, Balitactac N, Boone L and Litovitz T A 1971 *J. Chem. Phys.* **55** 3013
[6] Weiler R, Blaser S and Macedo P B 1969 *J. Phys. Chem.* **73** 4147
Tweer H, Laberge N and Macedo P B 1971 *J. Am. Ceram. Soc.* **54** 121
[7] Hasz W C, Whang J H and Moynihan C T 1993 *J. Non-Cryst. Solids* **161** 127
[8] Arkhipov S, Kashina N and Kuzina V 1973 *Russ. J. Inorg. Chem.* **18** 1675
[9] Hildebrand J H 1977 *Viscosity and Diffusion: a Predictive Treatment* (New York: Wiley)
[10] A line tangential to the high-temperature experimental data crosses the axis at the temperature T_ρ which characterizes the melt. On the other hand, the calculation of the point where the tangential line (at the inflection point of equation (2)) crosses the T/E_ρ axis gives the relation between T_ρ and E_ρ: $E_\rho/T_\rho = (3 + 2\sqrt{2}) \approx 5.83$, analogously to what has been shown for viscosity in reference [1, 2]. Thus the high-temperature activation energy E_ρ of the melt can be reasonably estimated from the linear part of the conductivity temperature dependence.
[11] Vogel H 1921 *Phys. Z.* **22** 645
[12] Angell C A 1991 *J. Non-Cryst. Solids* **13** 131
[13] Kauzmann W 1948 *Chem. Rev.* **43** 219
Adam G and Gibbs J H 1965 *J. Chem. Phys.* **43** 139
[14] Egelstaff P A 1992 *An Introduction to the Liquid State* (Oxford: Clarendon) p 268
[15] Hansen J-P and McDonald J R 1991 *Theory of Simple Liquids* (New York: Academic) p 399
[16] Voronel A, Veliyulin E, Machavariani V Sh, Kisliuk A and Quitmann D 1998 *Phys. Rev. Lett.* **80** 2630
[17] Pollack G 1981 *Phys. Rev.* A **23** 2660
Pollack G 1985 *Phys. Rev.* A **31** 980
[18] Chang I, Fujara F, Geil B, Heuberger G, Mangel T and Sillescu H 1994 *J. Non-Cryst. Solids* **172–174** 248
[19] Heber Green W 1908 *J. Chem. Soc.* **93** 2023
[20] Glotzer S C and Donati C 1999 *J. Phys.: Condens. Matter* **11** A285
[21] Yamamoto R and Onuki A 1998 *Phys. Rev.* E **58** 3515
[22] Götze W and Sjogren L 1996 *Chem. Phys.* **212** 47
[23] Andreozzi L, Di Schino A, Goirdano M and Leporini D 1997 *Europhys. Lett.* **38** 669
[24] Ghosh S S and Dasgupta C 1996 *Phys. Rev. Lett.* **77** 1310
Kob W, Donati C, Plimpton S J, Poole P H and Glotzer S C 1997 *Phys. Rev. Lett.* **79** 2827
[25] Stillinger F 1988 *J. Chem. Phys.* **89** 6461
Stillinger F and Hodgdon J 1994 *Phys. Rev.* E **50** 2064
[26] Kirkpatrick T, Thirumalai D and Wolynes P 1989 *Phys. Rev.* A **40** 1045
Chamberlin R and Kingsbury D 1994 *J. Non-Cryst. Solids* **172–174** 318
[27] Bendler J and Schlesinger M 1992 *J. Phys. Chem.* **96** 3970
[28] Kivelson S, Zhao X, Kivelson D, Fisher T and Knobler C 1994 *J. Chem. Phys.* **101** 2391
[29] Gerharz B, Meier G and Fisher E 1990 *J. Chem. Phys.* **92** 7110
Fisher E, Donth E and Steffen W 1992 *Phys. Rev. Lett.* **68** 2344
Patterson G and Stevens J 1994 *J. Non-Cryst. Solids* **172–174** 311
Steffen W, Patkowsky A, Meyer G and Fisher E W 1992 *J. Chem. Phys.* **96** 4171
[30] Cicerone M and Ediger M 1993 *J. Phys. Chem.* **97** 10 489
Cicerone M, Blackburn F and Ediger M 1995 *J. Chem. Phys.* **102** 471
Earl K, Moscicki J, Polimeno A and Freed J 1997 *J. Chem. Phys.* **106** 9996
[31] Bruggemann D A G 1935 *Ann. Phys., Lpz.* **24** 636
[32] Schwartz M and Edwards S F 1988 *Physica* A **153** 355
Schwartz M and Edwards S F 1990 *Physica* A **167** 595
Navot Y 1994 *Physica* A **210** 139
Navot Y and Schwartz M 1997 *Phys. Rev. Lett.* **79** 4786
[33] Nelson D 1983 *Phys. Rev. Lett.* **50** 982
Nelson D and Spaepen F 1989 *Solid State Physics* vol 42 (San Diego, CA: Academic) p 1
[34] Stauffer D and Aharony A 1992 *Introduction to Percolation Theory* (London: Taylor and Francis)